

Application of single-electron effects to fingerprints of chips

T. Tanamoto,¹ Y. Nishi,¹ and K. Ono²

¹Corporate R & D, Toshiba Corporation, Saiwai-ku, Kawasaki 212-8582, Japan*

²Advanced Device Laboratory, RIKEN, Wako-shi, Saitama 351-0198, Japan

(Dated: April 17, 2019)

Single-electron effects have been widely investigated as a typical physical phenomenon in nanoelectronics. The single-electron effect caused by trap sites has been observed in many devices. In general, traps are randomly distributed and not controllable; therefore, different current–voltage characteristics are observed through traps even in silicon transistors having the same device parameters (e.g., gate length). This allows us to use single-electron effects as fingerprints of chips. In this study, we analyze the single-electron effect of traps in conventional silicon transistors and show the possibility of their use as fingerprints of chips through image recognition algorithms. Resonant tunneling parts in the Coulomb diagram can also be used to characterize each device. These results show that single-electron effects can provide a quantum version of a physically unclonable function (quantum-PUF).

Single-electron tunneling (SET)^{1–14} is experimentally observed when electrons are confined in a small space and the number of electrons is countable. Since the 1990s, many studies have used SET to investigate Kondo effects^{15,16} and, more recently, quantum computing^{17–20}. Single-electron effects are also observed through trap sites in metal-oxide-semiconductor field-effect transistors (MOSFETs). The single-electron effect caused by a trap site is understandable when trap sites are regarded as quantum dots (QDs), that is, a confined region of electrons with discrete energy levels (Fig. 1). When a single QD is weakly coupled to both the source and the drain electrodes and capacitively coupled to the gate electrode, the measurement of the drain current I_D as a function of source voltage V_S and gate voltage V_G reveals a series of diamond-shaped regions where I_D is strongly suppressed. The features of the diamond-shaped regions, called Coulomb diamonds (CDs), indicate the threshold characteristics of SET. The size of the CD measured in V_S is the energy of Coulomb charging and/or quantum confinement for the dot. When more than two trap sites are coupled to the source and drain electrodes and contribute to SET, the CD shows a more complicated pattern comprising jagged corner lines²¹. Such complicated CD patterns represent the details of single-electron transport in multiple-QD devices^{2,6,8,18}.

Because the spatial positions, density, and energy levels of trap sites are not controllable, the features of CDs can differ in devices produced by the same fabrication processes. Therefore, one application of single-electron effects is the use of CDs as a “fingerprint” of devices.

In general, the fingerprint of a device can be considered a physically unclonable function (PUF) if it is unique, unclonable, and reliable. Emerging Internet of Things (IoT) technologies require a stable security system to protect users’ personal information. PUFs are considered an important mechanism for providing a unique and inexpensive identification (ID) for each device. A PUF outputs a response ID when a challenge signal is inputted from a server or an authorized system. PUF signals mostly originate from process variations of transistors and circuits. Basic static random access memory (SRAM) consists of two cross-coupled inverters and has fixed memory values only after a 0 or 1 datum is inputted. Therefore, the initial memory value is determined by the threshold

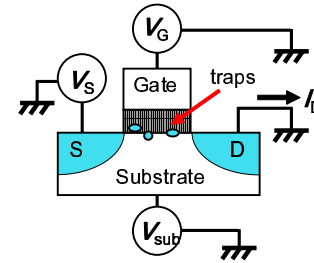


FIG. 1: Schematic of metal-oxide-semiconductor field-effect transistor (MOSFET) channel with three trap sites marked as small circles around the channel region. We measure the current between the source and the drain as we vary the source-drain (V_S), gate voltage (V_G), and substrate voltage (V_{sub}). Trap sites can be treated as quantum dots having discrete energy levels.

variations of the transistors; this is the operating principle of SRAM-PUF^{22,23}. The initial defects of memories^{24,25} or the circuit delay^{26–28} can also be used for generating PUFs.

Roberts *et al.* investigated PUFs using the quantum phenomena of resonant tunneling²⁹. Škorić proposed a quantum readout PUF in which a classical PUF is changed by the quantum state of photons³⁰. Chen *et al.* proposed a PUF using traps in transistors (trap-PUF), in which the fingerprint of a chip is created by allocating 0 or 1 to each transistor depending on whether the trap site can be detected or not, respectively, in the range of the given voltage region³¹. In the trap-PUF, when a 128-bit ID is requested, at least 128 transistors and related amplifying circuits are needed. The individuality of chips in the trap-PUF is based on the fact that trap distributions cannot be controlled precisely using current fabrication technologies.

In this study, we aim to further extend the use of trap sites in PUFs by using the single-electron effect of traps. We use the features of CDs of traps as fingerprints of devices. When we use single-electron effects as a PUF, one transistor is expected to be sufficient for use as a fingerprint of the whole chip, thereby reducing the trap-PUF circuit area in the chip. We further propose using image-matching algorithms to identify different CDs of transistors. For this purpose, characteristic key points are abstracted by treating CDs as images as

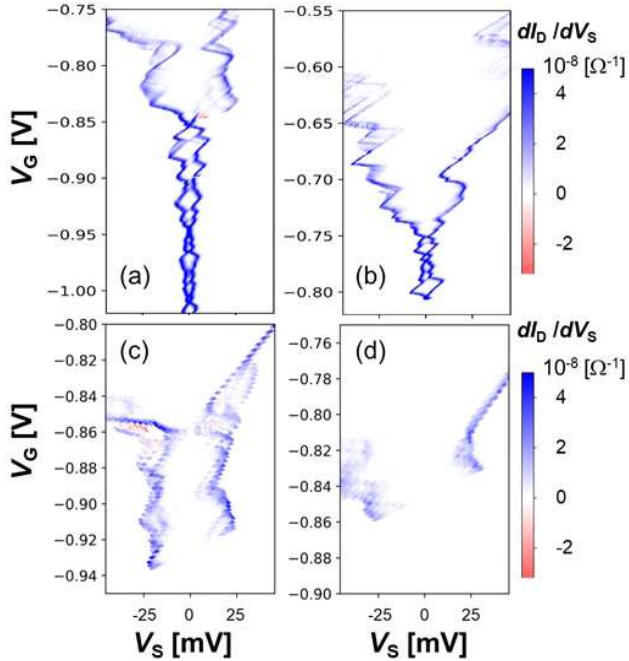


FIG. 2: dI_D/dV_S (differential conductance) characteristics of trap states in conventional 220-nm-wide transistors. In our measurement, $|I_D| > 120$ pA is not measured as values saturate in these regions. Thus, dI_D/dV_S is nominally zero (white color) in these regions. dI_D/dV_S is calculated from measured current I_D as a function of source voltage V_S . The operating temperature in this study is 1.54 K. (a) and (b) show the results for pMOSFETs having the same layout with 125-nm gate length. (c) and (d) show the results for pMOSFETs having the same layout with 125-nm gate length and a silicon oxynitride gate dielectric. Although these two devices have the same layout parameters (L and W), their CDs show different characteristics and can therefore be used to identify each device.

in conventional human fingerprint detection. We demonstrate that this approach simplifies the identification process.

We prepared conventional p-type metal-oxide-semiconductor field-effect transistors (pMOSFETs) fabricated on our prototype production line. These pMOSFETs have gate length $L = 125$ – 145 nm and fixed gate width $W = 220$ nm. Coulomb blockade is observed at low temperature, and it disappears as the temperature increases to room temperature. Figure 2 shows examples of the output of dI_D/dV_S through trap sites in pMOSFETs with $L = 125$ nm. As a reference, the average threshold voltage variations of transistors with $L = 125$ – 135 nm are generally calculated in the range of 25–50 mV³². Figure 2(a) and (b) show the results for wafers with identical L and W that were simultaneously fabricated with the same process conditions. Figure 2(c) and (d) show the results for wafers with identical L and W and an additional silicon oxynitride layer in the gate layer but fabricated with different process conditions.

Trap sites, which are often defects, are generally removed to the greatest extent possible because they cause undesirable noises and nonuniformity in device characteristics. These trap

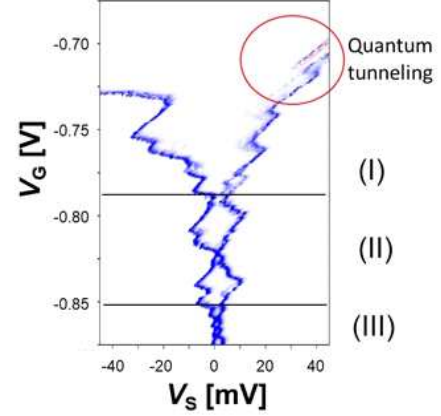


FIG. 3: Most CD images can be separated into three regions based on the physical tunneling mechanism. Region (I): Sub-threshold region. Region (II): Coulomb blockade caused by a couple of traps. Region (III): Coulomb blockade caused by many traps. The blue part shows $dI_D/dV_S > 0$. The red part shows $dI_D/dV_S < 0$ where we consider that resonant tunneling occurs. The quantum region (resonant tunneling region) is mainly observed in region (III).

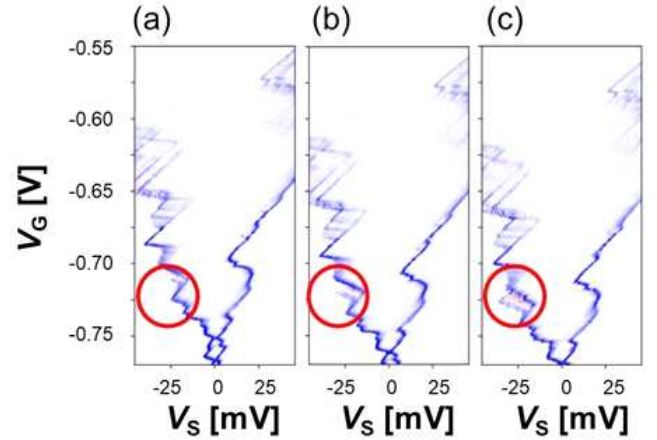


FIG. 4: CD image changes when substrate voltage V_{sub} changes. The differential conductance is measured in a conventional pMOSFET with 220-nm width and 125-nm length. (a) $V_{\text{sub}} = 0.0$ V, (b) $V_{\text{sub}} = 0.05$ V, and (c) $V_{\text{sub}} = 0.1$ V. The red circles show an example of a changed part with different V_{sub} .

sites are constructed at an atomic level; therefore, their CDs are uncontrollable and unclonable by current CMOS technologies. Thus, even if we fabricate transistors in the same product line, the features of the Coulomb blockade caused by single-electron effects can serve as a unique ID for each device. A CD image is obtained by measuring the current I_D as a function of gate voltage V_G and source voltage V_S and then numerically estimating the differential conductance dI_D/dV_S .

We divide the experimental data into three regions based on their different physical mechanisms of Coulomb blockade. As seen in Fig. 3, CD images can be divided into three parts de-

pending on the magnitude of the gate bias. Region (I): When V_G is low, the current flows exponentially as a function of drain voltage. Region (II): When V_G is applied beyond the subthreshold region, the current increases linearly as a function of V_S . Region (III): When V_G is sufficiently large, the current saturates. Regions (I) and (III) correspond to the subthreshold and saturation region of conventional MOSFET operation, respectively. In the subthreshold region, we can see the quantum aspect of the SET. Without quantum effects, the I_D - V_S characteristics show a step structure. This results from classical Coulomb blockade in which the current is hindered until the applied voltage exceeds the potential at which the next energy level is occupied.

The CD images in Figs. 2 and 3 have many similar jagged corner lines. These features make identification difficult if we compare CD images numerically using conventional data such as $(V_S, V_G, dI_D/dV_S)$. In ID applications, unstable output values are not desirable. However, the output signals of devices do not always have identical values. Devices degrade owing to aging effects caused by negative bias temperature instability (NBTI)³⁶. When a chip is powered by a battery, the voltages applied to the electrode probably fluctuate even when a voltage regulator is used. Thus, the current-voltage (I - V) characteristics will likely change every time the devices are measured. The electronic states of QD devices are generally affected by both V_{sub} and V_G values. A change in V_{sub} changes the energy levels of trap sites and the carrier densities of electrodes, resulting in changes in CD images. Therefore, we can emulate the effects of device conditions by changing V_{sub} .

Figures 4 show CD images of a pMOSFET with $L = 135$ nm and $W = 220$ nm when the substrate bias V_{sub} changes from 0.0 to 0.1 V. The details of the CD images clearly change with changes in V_{sub} . Two transistors can be distinguished successfully if the two CD images can be distinguished under changes in V_{sub} . For example, in the detection of human fingerprints, the surface condition of human fingers changes depending on both internal and external conditions such that human fingers are sometimes wet and sometimes oily. However, fingerprints should be identified every time they are measured. To identify fingerprints, key points in images of fingers are detected and compared with the image stored in the database. Similarly, detecting key points should be effective for finding the similarity of CD images. Although error-correction methods such as fuzzy algorithms can be used for this purpose³⁷, we propose a direct method to find the similarity and difference by regarding measurement data as images. Then, experimental data can be compared more flexibly using images in a manner similar to comparing human fingerprints or pictures.

Many advanced recognition algorithms have been developed for feature detection and image matching over the years^{38,39}. Image matching software usually detect three image features: edge, corner, and flat. An edge is a line or border at which a surface terminates, a corner is a place where two converging lines or surfaces meet, and a flat is a surface without any structures or marks. We apply the AKAZE⁴⁰, BRISK⁴¹, and ORB⁴² recognition algorithms to obtain the key points of CD images. AKAZE⁴⁰ algorithm uses a non-

linear diffusion filtering technique whose scale spaces are constructed using a computationally efficient mathematical framework called fast explicit diffusion (FED). ORB⁴² is an extended algorithm using other algorithms that is rotation-invariant and noise-resistant. In the BRISK algorithm, key points are detected in octave layers of the image pyramid as well as in in-between layers, and the sampling pattern consists of concentric circles in the neighborhood of each key point. In this study, we used Open Source Computer Vision Library (OpenCV ver.3)⁴³ based on Python 3. The main advantage of using image matching software is that we can express the difference between two images by a single numerical value called *distance* that is obtained as the output of each algorithm.

Figures 5 show an example of the extraction of characteristic key points between the two CD images of the same device ((a) and (b)) and different devices ((c) and (d)). The connected lines between key points in Figs. 5(a) and (b) look more condensed than those in Figs. 5(c) and (d). To understand the statistical characteristics, it is better to use histograms. Figure 6 shows histograms of the *distances* between the two CD images. The blue and yellow data show the distributions of the same and different devices, respectively, with different V_{sub} s. The results show that the two devices can be distinguished by calculating the *distance* of two CD images. Each recognition algorithm has its own specific parameters such as a threshold and number of feature points. As long as we chose several sets of parameters, we could not see any prominent improvement for some specific parameter sets. Thus, we used the default parameters of each algorithm. The two peaks in the distributions of the same devices (Figs. 6 (b) and (c)) are considered to originate from some detailed data structure in the same devices; we cannot explain the reason at present. Figure 7 shows histograms of the *distances* between the two CD images for devices with different L s. The *distances* in devices with the same L s are clearly smaller than those in devices with different L s, and we can distinguish device IDs by using the CD images.

Single-electron effects include various quantum tunneling processes such as cotunneling³⁻⁵. Here, we simply investigate quantum effects where dI_D/dV_S has negative values. This is the result of resonant tunneling effects using the discrete energy levels of trap sites. Figure 8 shows histograms over data of negative differential conductance ($dI_D/dV_S < 0$) for two transistors with $L = 125$ nm and $W = 220$ nm. Each figure includes several distributions of the negative differential conductance with different V_{sub} s in the range of ± 0.1 V. The histogram is divided into 50 regions in each of which values of the standard deviation are divided by their average. The calculated deviation resulting from V_{sub} variations is 0.176% for Fig. 8(a) and 0.385% for Fig. 8(b). The relative difference of the two transistors is calculated by

$$\frac{|\text{Average}(\text{Fig. (a)}) - \text{Average}(\text{Fig. (b)})|}{|\text{Average}(\text{Fig. (a)}) + \text{Average}(\text{Fig. (b)})|/2} = 0.83\%. \quad (1)$$

Thus, although the difference is not large, the histogram of the quantum part also helps to distinguish the different transistors.

In this study, CDs are measured at cryogenic temperatures.

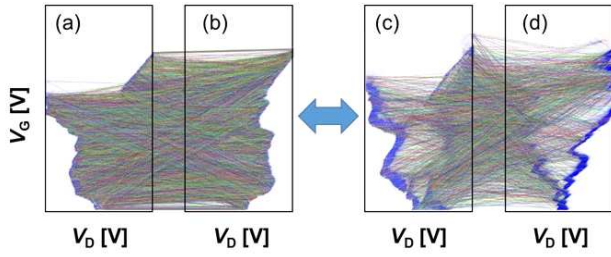


FIG. 5: Examples of extraction of key points from CD images in regions (I) and (II) using AKAZE recognition algorithm. The distance between (a) and (b) is 46.52 ($V_{sub} = 0.5$ V and 0.6 V) and that between (c) and (d) is 95.40 ($V_{sub} = 0.1$ V and 0.14 V). pMOSFETs with $L = 125$ nm.

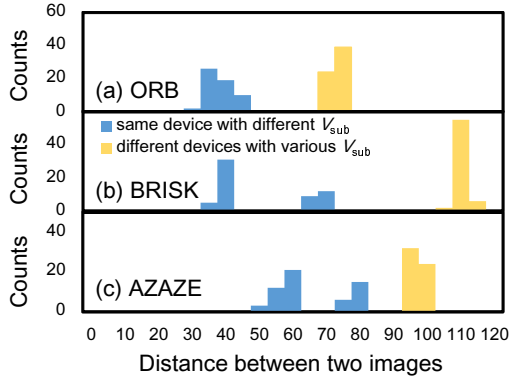


FIG. 6: Comparison of histograms of distances of two images using three recognition algorithms ((a) ORB, (b) BRISK, and (c) AKAZE) for changing V_{sub} s. The scan region is restricted to 0.15 V. “Same device” shows the results for different V_{sub} s with the same devices. “Different device” shows the results for different V_{sub} s with different devices.

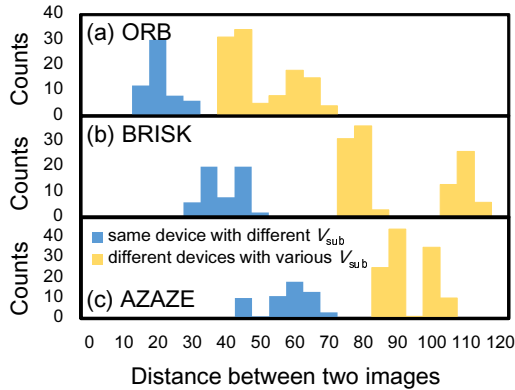


FIG. 7: Comparison of histograms of distances of two images using three recognition algorithms ((a) ORB, (b) BRISK, and (c) AKAZE) for changing V_{sub} s. Devices with $L = 125$ nm, $L = 135$ nm, and $L = 140$ nm are measured.

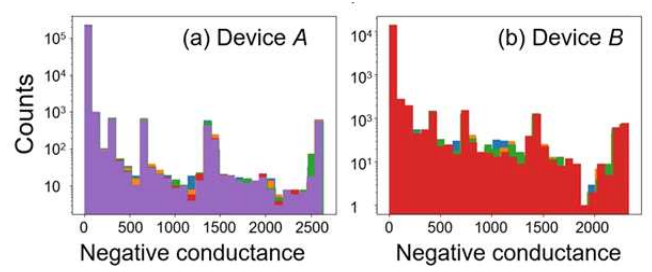


FIG. 8: Histogram of differential conductance $dI_D/dV_S < 0$ data in two devices *A* and *B* with $L = 125$ nm and $W = 220$ nm). We can see differences between two devices even if they are made as the same transistors. The different colors corresponds to various V_{sub} s.

Note that single-electron effects can be observed even at room temperature if the device is designed appropriately^{33–35}. However, this requires additional fabrication processes and incurs higher cost. There is a trade-off between the fabrication cost and the operating temperature. In this study, the number of tested transistors with the same L and W is limited because of the limited fabrication resources for wafers. The main purpose of this study was to present the concept of a quantum PUF in single-electron devices. An examination of many transistors will be performed in a future study.

In summary, we have proposed a quantum PUF based on single-electron devices. In particular, we showed that we can distinguish two devices by using the distances calculated from CD images. In contrast with the trap-PUF³¹ in which many transistors need to be measured, only one transistor is needed to generate the fingerprint of the chip, and thus, the number of devices to be measured is greatly reduced. Note that electrons in traps can be treated as spin-qubits¹⁸. Because trap distributions differ depending on the transistor, corresponding spin-qubit behaviors are also expected to differ depending on the transistor. Thus, the quantum behavior of an electron in a trap site can also be used as a fingerprint of a chip. This will be explored in a future study.

Acknowledgement

TT thanks T. Hiraoka and T. Hioki for useful discussions.

* Present Address Teikyo University.; Electronic address: tanamoto@ics.teikyo-u.ac.jp

¹ D. V. Averin and K. K Likharev, in Mesoscopic Phenomena in

- Solids, eds. B. L. Altshuler, P. A. Lee, and R. A. Webb (Elsevier, Amsterdam, 1991)
- ² L. P. Kouwenhoven, C. M. Marcus, P. L. McEuen, S. Tarucha, R. M. Westervelt, and N. S. Wingreen, in *Mesoscopic Electron Transport*, eds. L. L. Sohn, G. Schon, L. P. Kouwenhoven (Kluwer, Dordrecht, Netherlands, Series E345, 1997).
 - ³ D. V. Averin and Yu. V. Nazarov, *Phys. Rev. Lett.* **65**, 2446 (1990).
 - ⁴ L. J. Geerligs, D. V. Averin, and J. E. Mooij, *Phys. Rev. Lett.* **65**, 3037 (1990).
 - ⁵ T. M. Eiles, G. Zimmerli, H. D. Jensen, and J. M. Martinis, *Phys. Rev. Lett.* **69**, 148 (1992).
 - ⁶ H. Sellier, G. P. Lansbergen, J. Caro, S. Rogge, N. Collaert, I. Ferain, M. Jurczak, and S. Biesemans, *Phys. Rev. Lett.* **97**, 206805 (2006).
 - ⁷ Y. Ono, K. Nishiguchi, A. Fujiwara, H. Yamaguchi, H. Inokawa, and Y. Takahashi, *Appl. Phys. Lett.* **90**, 102106 (2007).
 - ⁸ G. P. Lansbergen, R. Rahman, C. J. Wellard, I. Woo, J. Caro, N. Collaert, S. Biesemans, G. Klimeck, L. C. L. Hollenberg, and S. Rogge, *Nat. Phys.* **4**, 656 (2008).
 - ⁹ K. Y. Tan et al., *Nano Lett.* **10**, 11 (2010).
 - ¹⁰ M. Pierre, R. Wacquez, X. Jehl, M. Sanquer, M. Vinet, and O. Cueto, *Nat. Nanotechnol.* **5**, 133 (2010).
 - ¹¹ M. F. Gonzalez-Zalba, A. Saraiva, M. J. Calderón, D. Heiss, B. Koiller, and A. J. Ferguson, *Nano Lett.* **14**, 5672 (2014).
 - ¹² R. Schleser, T. Ihn, E. Ruh, K. Ensslin, M. Tews, D. Pfannkuche, D. C. Driscoll, and A. C. Gossard, *Phys. Rev. Lett.* **94**, 206805 (2005).
 - ¹³ M. Sigrist, T. Ihn, K. Ensslin, M. Reinwald, and W. Wegscheider, *Phys. Rev. Lett.* **98**, 036805 (2007).
 - ¹⁴ K. Ono, T. Tanamoto, and T. Ohguro, *Appl. Phys. Lett.* **103**, 183107 (2013).
 - ¹⁵ D. Goldhaber-Gordon, H. Shtrikman, D. Mahalu, D. Abusch-Magder, U. Meirav, and M. A. Kastner, *Nature* **391**, 156 (1998).
 - ¹⁶ J. Park, A. N. Pasupathy, J. I. Goldsmith, C. Chang, Y. Yaish, J. R. Petta, M. Rinkoski, J. P. Sethna, H. D. Abruña, P. L. McEuen, and D. C. Ralph, *Nature* **417**, 722 (2002).
 - ¹⁷ J. J. Pla, K. Y. Tan, J. P. Dehollain, W. H. Lim, J. J. L. Morton, D. N. Jamieson, A. S. Dzurak, and A. Morello, *Nature* **489**, 541 (2012).
 - ¹⁸ K. Ono, G. Giavaras, T. Tanamoto, T. Ohguro, X. Hu, and F. Nori, *Phys. Rev. Lett.* **119**, 156802 (2017).
 - ¹⁹ T. Tanamoto, Y. Higashi, and J. Deguchi, *J. Appl. Phys.* **124**, 154301 (2018).
 - ²⁰ T. Tanamoto, Y. Nishi, and J. Deguchi, *J. of Phys. Soc. Jpn.* **88**, 061013 (2019).
 - ²¹ I. M. Ruzin, V. Chandrasekhar, E. I. Levin, and L. I. Glazman, *Phys. Rev. B* **45**, 13469 (1992).
 - ²² J. Guajardo, S. S. Kumar, G.-J. Schrijen, and P. Tuyls, *Proc. 9th Int. Workshop on Cryptographic Hardware and Embedded Systems (CHES'07)*, 2007, pp. 63-80.
 - ²³ D. E. Holcomb, W. P. Burlison, and K. Fu, *IEEE Trans. Comput.* **58**, 1198 (2009).
 - ²⁴ T. Marukame, T. Tanamoto, and Y. Mitani, *IEEE Trans. Mag.* **50**, 1 (2014).
 - ²⁵ A. Chen, *IEEE Elec. Dev. Lett.* **36**, 138 (2015).
 - ²⁶ D. Lim, J. Lee, B. Gassend, G. Suh, M. van Dijk, and S. Devadas, *IEEE Trans. Very Large Scale Integr. (VLSI) Syst.* **13**, 1200 (2005).
 - ²⁷ G. E. Suh and S. Devadas, *Proc. 44th Ann. Design Automation Conf. (DAC'07)*, 2007, pp. 9-14.
 - ²⁸ T. Tanamoto, S. Yasuda, S. Takaya and S. Fujita, *IEEE Trans. Circuits and Systems II: Express Briefs* **64**, 827-831 (2017).
 - ²⁹ J. Roberts, I. E. Bagci, M. A. M. Zawawi, J. Sexton, N. Hulbert, Y. J. Noori, M. P. Young, C. S. Woodhead, M. Missous, M. A. Migliorato, U. Roedig, and R. J. Young, *Sci. Rep.* **5**, 16456 (2015).
 - ³⁰ B. Škorić, *Int. J. of Quantum Information* **10**, 1250001 (2012).
 - ³¹ J. Chen, T. Tanamoto, H. Noguchi, and Y. Mitani, *2015 IEEE Symp. VLSI Tech.* 2015, pp. 40-41.
 - ³² A. Asenov, *IEEE Trans. Electron Devices* **45**, 2505-2513 (1998).
 - ³³ K. Uchida, J. Koga, R. Ohba, and A. Toriumi, *IEEE Trans. Electron Devices* **50**, 1623 (2003).
 - ³⁴ Y. T. Tan, T. Kamiya, Z. A. K. Durrani, and H. Ahmed, *J. Appl. Phys.* **94**, 633 (2003).
 - ³⁵ V. Ray, R. Subramanian, P. Bhadrachalam, L.-C. Ma, C.-U. Kim, and S. J. Koh, *Nature Nanotechnology* **3**, 603 (2008).
 - ³⁶ R. Vattikonda, W. Wang, and Y. Cao, *Proc. IEEE Des. Autom. Conf.* 1047 (2006).
 - ³⁷ Y. Dodis, R. Ostrovsky, L. Reyzin, and A. Smith, *SIAM Journal on Computing* **38**, 97 (2008).
 - ³⁸ Z. Peng, "Efficient matching of robust features for embedded SLAM," *Computer Science*, University of Stuttgart, 2012.
 - ³⁹ S. Isik and K. Ozkan, *International Journal of Applied Mathematics, Electronics and Computers* **3**, 1 (2015).
 - ⁴⁰ P. F. Alcantarilla, J. Nuevo, and A. Bartoli, *textitProc. British Machine Vision Conference (BMVC)*, Bristol (2013).
 - ⁴¹ S. Leutenegger, M. Chli, and R. Siegwart, *Proc. Int. Conf. Computer Vision* 2548 (2011).
 - ⁴² E. Rublee, V. Rabaud, K. Konolige, and G. Bradski, *textitIEEE International Conference on Computer Vision (ICCV)*, Barcelona, 2564 (2011).
 - ⁴³ <https://opencv.org/>

